Reactions in non-aqueous alkali and alkaline-earth metal-oxygen batteries: a thermodynamic study

Adriano Pierini,[1] Sergio Brutti[1,2] and Enrico Bodo[1,*]

[1]Department of Chemistry, University of Rome "La Sapienza", P. A. Moro 5, 00185 Rome, Italy

[2]GISEL—Centro di Riferimento Nazionale per i Sistemi di Accumulo Elettrochimico di Energia, INSTM, via G. Giusti 9, 50121 Firenze, Italy

*Corresponding author, e-mail: enrico.bodo@uniroma1.it

Abstract

Multivalent aprotic metal-oxygen batteries are a novel concept in the applied electrochemistry field. These systems are variants of the so-called Li-air batteries and up to present are in their research infancy. The superoxide disproportionation reaction is a crucial step for the operation of any metal-oxygen redox system using aprotic solvents: in the best scenario, disproportionation leads to peroxide formation while in the worse one it releases singlet molecular oxygen. In this work we address the fundamental thermodynamics of such reaction for alkali (Li, Na and K) and alkaline earth (Be, Mg and Ca) metal-O_2 systems using multiconfigurational ab-initio methods. Our aim is to draw a comprehensive description of the disproportionation reaction from superoxides to peroxides and to provide the thermodynamic likelihood of the pathways to singlet oxygen release.

Keywords: metal-oxygen batteries; aprotic batteries; ab initio thermodynamics; alkaline earth metals;

1 Introduction

Aprotic Metal-O_2 (air) batteries based on Li, Na, and K are experiencing in recent years extraordinary research efforts, motivated by their theoretical energy density, better sustainability and lower costs compared to current state-of-the-art technologies.[1–3] Very recently Mg- and Ca-O_2 battery chemistries have been also proposed in view of the good theoretical properties (957 and 742 $mAhg^{-1}$ for the MgO_2 and CaO_2 reversible electrochemistry, respectively), of the environmental benignity of the chemical species and of the wide availability of Mg and Ca.[4–7] Generally speaking, aprotic metal-O_2 secondary galvanic cells are constituted by (i) a porous positive electrode (e.g. nanoscaffolded carbons) where the gaseous O_2 is reduced and oxidized reversibly, (ii) a metal negative electrode (e.g. Li, Na, K, Mg, Ca) where reversible plating/stripping redox reactions occur and (iii) a non-aqueous electrolyte constituted by an organic solvent (e.g. glymes, short chain and cyclic ethers, sulphones, ionic liquids) and an inorganic salt (e.g. lithium bis(trifluoromethane)-sulphonil-imide, sodium perchlorate). In all these energy storage devices, (ir)-reversible formation/decomposition of metal superoxides/peroxides/oxides at the positive electrode on discharge/charge is critically important.[3]

Overall, the development of metal-O_2 batteries suffer a poor understanding of the fundamental electrochemical reactions at molecular level that drive the reversible redox reactions at electrodes, as well as irreversible parasitic processes.[3,8–11]

Researchers are still puzzled by the difficulties experienced in the actual implementations vis-a-vis the apparent simplicity of the electrochemical processes that drive secondary non-aqueous metal-oxygen batteries (e.g. Li-, Na-, K-, Mg- and Ca-O_2) that are summarized in the following reactions for an alkali metal Am-O_2 case:[2]

$$\mathrm{Am^+(solvated) + e^- + O_2(gas) \rightarrow AmO_2(solvated\ or\ solid)} \quad \text{(R1)}$$

$$\mathrm{2Am^+(solvated) + 2e^- + O_2(gas) \rightarrow Am_2O_2(solvated\ or\ solid)} \quad \text{(R2)}$$

$$\mathrm{4Am^+(solvated) + 4e^- + O_2(gas) \rightarrow 2Am_2O(solvated\ or\ solid)} \quad \text{(R3)}$$

Generally speaking, the nucleation and growth of metal superoxides/peroxides/oxides on the surface of porous conductive electrodes is the key-point. However, the step-by-step reaction mechanism is complex and, up to now, its understanding at the molecular level has been thoroughly tackled only in the case of Li-O_2 batteries. In particular, since the electrochemical formation of Li_2O

is irreversible, the Li-O_2 batteries electrochemistry is hampered by the formation of superoxide/peroxide monomers and oligomers in solution and their subsequent precipitation onto the electrode surfaces and by a complex interplay between electrochemical and chemical processes.[11–15] As a consequence, it is now commonly accepted that an effective operation of Li-O_2 batteries is strongly affected by the nature and solvation properties of the electrolytes as well as the ability of the lithium ions to coordinate anions and solvent molecules in solution.[14,16] Similar consolidated understandings are currently missing for all the other alkaline and alkaline-earth metal-oxygen battery chemistries.

On the other hand, a wide number of literature papers suggests a poor selectivity of the electrochemical peroxide and superoxide formation/dissolution reaction in Li-O_2 cells due to competitive chemistries.[17–19]

The simplest competitive reaction is the disproportionation of the metal superoxides to form peroxides and release molecular oxygen:

$$2\mathrm{AmO_2} \rightarrow \mathrm{Am_2O_2} + \mathrm{O_2(gas)} \qquad \text{(R4)}$$

This reaction has been demonstrated computationally and experimentally in the case of Li-O_2 and Na-O_2 systems[20–24] and this evidence suggests the remarkable role of protons and weak Lewis acids to boost its kinetic. Furthermore, the disproportionation R4 can lead to the release of singlet molecular oxygen, a highly-reactive specie that can onset degradation reactions in any chemical system.[24]

The most studied chemistries that compete with the peroxide and superoxide electrochemical formation/dissolution reaction are the parasitic degradation processes that waste the electrolyte and electrode components in the battery. Although the reactivity of (su)peroxides was held responsible,[9] the nucleophile character of this molecule cannot conclusively explain the observed irreversible processes and degradation of the electrolyte.[10] Specifically, it cannot explain why reactivity would seemingly grow in the order KO_2 < NaO_2 < LiO_2, and why superoxides were less reactive than peroxides.[16] Recently, the formation of singlet molecular oxygen ($^1O_2$), experimentally identified as intermediate species in Li-O_2 and Na-O_2 batteries,[25–28] has been held responsible for the onset of the degradation chemistry upon cycling.[23,24]

Turning to alkaline earth metals (Ae)-O_2 cell, three half-reactions can be easily written on paper to describe the reduction reactions at the positive electrode in line to reactions 1-3:[4,6]

$$\mathrm{Ae^{2+}(solvated) + 2e^- + 2O_2(gas) \rightarrow Ae(O_2)_2(solvated\ or\ solid)} \quad \text{(R5)}$$

$$\mathrm{Ae^{2+}(solvated) + 2e^- + O_2(gas) \rightarrow AeO_2(solvated\ or\ solid)} \quad \text{(R6)}$$

$$\mathrm{Ae^{2+}(solvated) + 2e^- + \frac{1}{2}O_2(gas) \rightarrow AeO(solvated\ or\ solid)} \quad \text{(R7)}$$

In the case of Mg these reactions have thermodynamic redox potentials ranging between 3.0 and 2.9 V vs Mg^{2+}/Mg,[6,7] whereas in the case of Ca the standard Nernst potentials are in the range 3.3-3.0 V vs Ca^{2+}/Ca.[4,5] However these fundamental thermodynamic evaluations reported in the literature miss to tackle the complex solution/surface mediated chemistry/electrochemistry that, similarly to the case of the Li-O_2 cells, drives the reaction mechanism at molecular level. Baltruschat and co-workers[29] have recently suggested the possibility of singlet oxygen evolution from Ca^{2+}-driven superoxide disproportionation in DMSO. Nonetheless, there is still an almost complete lack of analysis, either experimental or computational, of both the disproportionation reaction and the degradation chemistry of non-aqueous electrolytes in both the Mg- and Ca-O_2 battery environments.

In this study we address a part of the fundamental thermodynamic properties of the superoxide disproportionation reaction by multiconfigurational ab initio methods for alkali and alkaline earth metal systems. To understand the likelihood of the disproportionation reaction of the superoxide to peroxide and molecular oxygen, we consider the following three reactions.

$$\mathrm{AmO_2 + AmO_2 \rightarrow [Am_2O_4] \rightarrow Am_2O_2 + O_2} \quad \text{(R8)}$$

$$\mathrm{AmO_2 + O_2^- \rightarrow [AmO_4]^- \rightarrow AmO_2^- + O_2} \quad \text{(R9)}$$

$$\mathrm{AeO_2^+ + O_2^- \rightarrow [AeO_4] \rightarrow AeO_2 + O_2} \quad \text{(R10)}$$

where the first two apply to alkali metals and the third one to alkaline-earth ones. Reactions R8 and R10 are expressed using an overall neutral chemistry, while R9 assumes a negatively charge state. The need for such high-level treatment of the energies stems from the inherent multistate nature of the above reactions and from the multiconfigurational character of the species involved.

2 Methods

The calculations have been carried out with the ORCA[30] code and with the augmented triple-ζ ma-def2-TZVP basis set. The geometries of the ground state molecules were optimized using the spin-component-scaled version of MP2 perturbation theory (SCS-MP2)[31]. In order to properly account for the diradical nature of some of the species and to determine accurate energies of the electronic

states, multi-reference correlated n-electron valence state perturbation theory (NEVPT2)[32,33] has been used at the MP2 geometries.

The strongly-contracted NEVPT2 energies were calculated on-top of a CASSCF wavefunction whose active space span over all of the valence p electrons and orbitals from the oxygen atoms. This leads for the larger systems containing 4 oxygen atoms to an (18,12) complete active space. Obviously, this active space has been consistently reduced for the smaller species containing only two oxygen atoms. In these cases, to obtain consistent thermodynamic data, the energy of an isolated $O_2(^3\Sigma)$ or $O_2(^1\Delta)$ molecule at the same computational level was added to that of the peroxide molecules. For the systems containing only one metal cation, the same NEVPT2 calculations have been repeated with an extended (18,13) active space which also contained the valence *s* orbital of the cation. The results obtained in this way are in perfect agreement with the previous ones, showing that the inclusion of the *s* orbitals is not important for the present results (for a study of the possible role of the *s* orbital occupation in a specific case see our study in ref. [34]). The reliability of the method has been further tested in two ways: (i) the extension of the atomic basis was checked by repeating one of the calculations using a "quadruple-zeta" basis, but only minor changes were noticed; (ii) few selected MP2 geometries were checked against an analogous optimization performed with the CASSCF/NEVPT2 method, but, again, the changes were substantially irrelevant.

The Gibbs free energies (at 298 K) of the ground state stationary points were evaluated through the calculation of harmonic vibrational frequencies with numerical SCS-MP2 hessian, thus including the zero-point-energies.

The geometries along the reaction paths have been obtained using SCS-MP2 and the nudged elastic band method (NEB), with 12 intermediate "images" between the two optimized minima. The energies the first four electronic states for each of these geometries have been computed using the above NEVPT2 method on top of state-averaged CASSCF calculations over the 5 roots.

Most of the calculations were first performed in vacuum, and then repeated including approximate solvation effects by mean of the implicit solvation model based on solute electron density (SMD) by Cramer and Truhlar,[35] using two different parametrized solvents (acetonitrile and diethyl ether). The optimized MP2 geometries were relaxed in the SMD solvents. The choice of these two model solvents is simply motivated by the need of having exemplar data for the two ends of the range of the typical dielectric constant values of the solvent actually employed in experimental setups.

3 Results and discussion

The thermodynamics in the gas and solution phases of the disproportionation reactions R8, R9 and R10 are summarized in tables 1, 2 and 3 respectively where NEVPT2 correlated multiconfigurational reaction energies are reported for alkaline and alkaline-earth metals.

3.1 The alkali metal electronic energies

For the alkali metals, reaction R8 (Table 1) is an overall neutral process where we associate two doublet superoxide neutral molecules (AmO_2). The association leads to the formation of a very stable complex (Am_2O_4) whose formation is always greatly exoergic. Since superoxide is a radical doublet, the two unpaired spins can organize themselves in a singlet or triplet multiplicity.

Table 1: NEVPT2/CASSCF energies for reaction R8. The data are reported for the triplet (ground state) multiplicity (normal fonts) and for the singlet multiplicity (excited state, bold fonts). All energies are referred to the reactant's energy: $AmO_2 + AmO_2$.

Am cation	Solvation	Am_2O_4	$Am_2O_2\cdots O_2$	$Am_2O_2 + O_2$
Li^+	gas	-1.52/**-1.51**	-0.82/**+0.14**	-0.79/**+0.17**
	Et_2O	-0.91/**-0.91**	-	-0.30/**+0.66**
	CH_3CN	-0.71/**-0.70**	-	-0.14/**+0.82**
Na^+	gas	-1.77/**-1.77**	-0.34/**+0.61**	-0.29/**+0.67**
	Et_2O	-1.07/**-1.07**	-	+0.24/**+1.20**
	CH_3CN	-0.82/**-0.82**	-	+0.40/**+1.36**
K^+	gas	-1.31/**-1.31**	+0.08/**+1.04**	+0.09/**+1.05**
	Et_2O	-1.18/**-1.18**	-	+0.62/**+1.58**
	CH_3CN	-0.94/**-0.94**	-	+0.79/**+1.75**

The energetic difference between the singlet and triplet electronic states in Am_2O_4 is negligible with respect to the energies at play in the reaction. Hence the energies of the singlet and triplet variants of Am_2O_4 are essentially the same as clearly shown in Table 1 third column. The Am_2O_4 complex can undergo disproportionation: one unpaired electron on the superoxide moiety (O_2^-) is transferred to the other superoxide, creating a peroxide (O_2^{2-}) and a neutral oxygen molecule. Along the reaction coordinate it is possible to identify a bound complex in the product region due to the weak

interaction of Am_2O_2 and O_2. We have found that the energetic location of this complex (Table 1, 4th column) is invariably very similar to the dissociated product state and we have computed it only for the gas-phase calculations. During the disproportionation process which is driven by a change in the O—O distances, the triplet and singlet variants become separated in energy by nearly 1 eV that is the singlet-triplet energy gap in O_2.

The geometric evolution of the O—O distance along the reaction path for the Li^+ case is reported in Figure 1 through the display of the structures corresponding to the stationary points along the potential energy surface. The reagent LiO_2 (neutral superoxide) is on the left. The O—O distance is 1.36 Å. Two superoxides associate to form the main reaction complex (middle of Figure 1) where the two O_2^- moieties have O—O distances that are typical of the superoxide (1.34 Å). Only when the final product is formed (the peroxide on the right of Figure 1), the O—O distance acquires the typical value of the peroxides (1.6 Å).

The overall disproportionation reaction leading to triplet oxygen is exoergic for Li^+ of -0.79 eV, a value that is reduced to -0.3/-0.14 eV when solvent effects are considered. Producing singlet oxygen, on the other hand, involves an endoergic chemical process and costs from 0.17 to 0.82 eV depending on the environment. For both Na^+ and K^+, the overall reaction profile becomes endoergic. The energy required to form the peroxide is moderate for Na^+ (+0.2/+0.4 eV) and higher for K^+ (+0.6/+0.8 eV). The formation of singlet oxygen for these two metals requires significantly more than 1 eV even when the reaction occurs in a solvent medium.

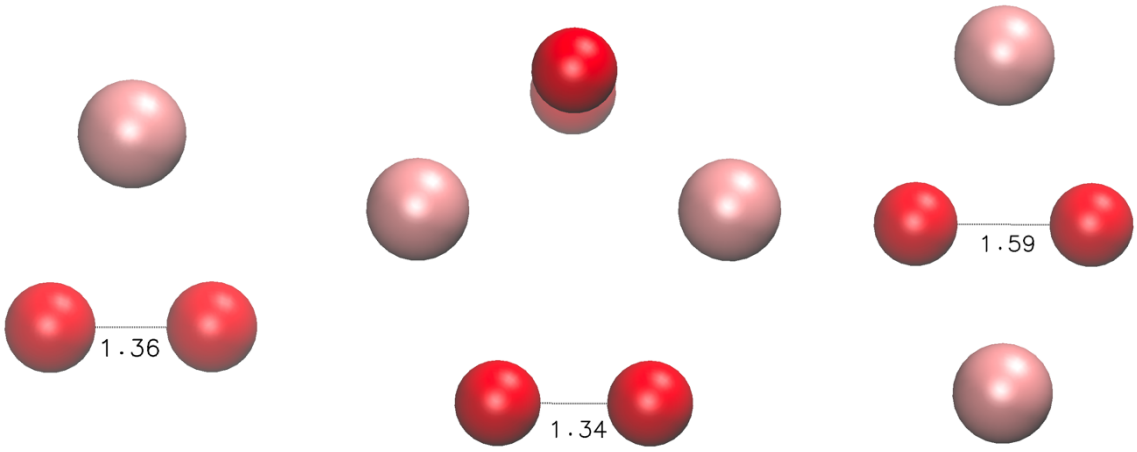

Figure 1: *MP2 geometries (in vacuo) of the stationary points along the R8 reaction for Li^+ (pink spheres). In reading order: LiO_2 (superoxide), Li_2O_4 (reaction complex), Li_2O_2 (peroxide).*

With respect to the gas-phase, the effect of the solvent is that of significantly reducing the energies differences of the reaction leading to Am_2O_2. The reduction in the formation of the Am_2O_4 complex is due to the association nature of the reaction, hence to the loss of one solvation shell. On the other hand, the energetic reduction of the entire reaction is likely due to the apolar nature of one of the final products (O_2) that determines a loss of solvation energy in the products with respect to the reactants.

The data in Table 2 pertain to the alkali metal reactions R9 where the thermodynamic has been computed using an anionic system with only one metal center.

Table 2: NEVPT2/CASSCF energies for reaction R9. The data are reported for the triplet (ground state) multiplicity (normal fonts) and for the singlet multiplicity (excited state, bold fonts). All energies are referred to the reactant's energy: $AmO_2 + O_2^-$.

Am cation	Solvation	AmO_4^-	$AmO_2^-\cdots O_2$	$AmO_2^- + O_2$
H^+	gas	-1.33/**-1.33**	-0.63/**+0.29**	-0.58/**+0.38**
	Et_2O	-0.92/**-0.93**	-	-0.57/**+0.39**
	CH_3CN	-0.27/**-0.28**	-	-0.56/**+0.40**
Li^+	gas	-2.66/**-2.66**	+0.55/**+1.51**	+0.64/**+1.60**
	Et_2O	-1.65/**-1.65**	-	+0.71/**+1.67**
	CH_3CN	-1.28/**-1.28**	-	+0.67/**+1.63**
Na^+	gas	-2.48/**-2.48**	+1.61/**+2.54**	+1.34/**+2.31**
	Et_2O	-1.39/**-1.39**	-	+1.24/**+2.20**
	CH_3CN	-1.01/**-1.01**	-	+1.11/**+2.07**
K^+	gas	-2.11/**-2.11**	+1.61/**+2.54**	+1.72/**+2.69**
	Et_2O	-1.08/**-1.08**	-	+1.53/**+2.49**
	CH_3CN	-0.73/**-0.73**	-	+1.35/**+2.31**

This system represents the simplest realistic model of the disproportionation reaction. For completeness we have also presented in Table 2 the data for the proton which is a very effective catalyzer of the disproportionation reaction as shown by us in ref[24]. The disproportionation reaction R9 is very efficient in presence of protons (hence any protic impurity) and exoergic of more than 0.5 eV regardless of solvent. The reaction R9 is instead endoergic for all three alkali metals and requires more energy than reaction R8. In its anionic form, the superoxide disproportionation is available only to Li^+ because the energy needed for heavier alkali largely exceeds 1 eV. Obtaining peroxides

from this reaction is increasingly difficult in the order $Li^+<Na^+<K^+$: for example, in diethyl ether the energies required to produce peroxides and triplet oxygen are +0.7, +1.2, +1.5 eV respectively.

As clearly shown in Table 2, the presence of a solvent environment has a significant effect on the energy of the association leading to AmO_4^-, but, overall, the dependence of reaction R9 on the solvent environment, is less evident than in the neutral reaction R8. Both reagents and products include one charged specie for which a similar stabilization occurs in the two SMD models. The evolution of the reaction complex in reaction R9 is illustrated in Figure 2 using Li^+ as an example. The geometries and distance are not dissimilar to the ones reported in Figure 1: as for the path illustrated for reaction R8, the process is driven by a change in the O—O distance of the O_2 moiety that remains bound to the metal (i.e., the one that is reduced).

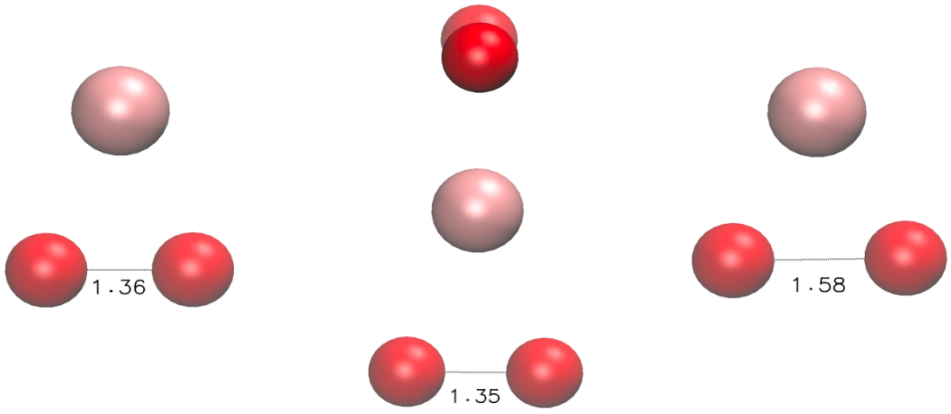

Figure 2: *MP2 geometries (in vacuo) of the stationary points along the R9 reaction for Li^+ (pink). In reading order: LiO_2 (superoxide), LiO_4^- (anionic reaction complex), LiO_2^- (peroxide anion).*

The mechanisms by which the superoxide reaction complex AmO_4^- transforms into a peroxide and a molecular oxygen via reaction R9 involves the intersection of two different electronic states. In order for the complex to reach the crossing point that has a high energy (similar to products), a geometric rearrangement is required. To illustrate the energetic path, we have identified the geometries along the reaction by tracing a possible minimum energy path using the nudged elastic band method. On top of these geometries, we have used the CASSCF/NEVPT2 methods to obtain the energies of the first relevant electronic states. The change in geometry along the reaction path is illustrated in a pictorial way in Figure 3 where we have sketched a generic AmO_4^- complex whose geometry (see Figure 2, middle panel) consists in two superoxides arranged perpendicularly to each other surrounding the central cation. The disproportionation reaction takes place when one of the O—O distance is reduced toward that of the neutral molecule and the other is increased to the

peroxide one. When the O—O distances changes, the central cation makes an arc motion from the center of the complex to one of its sides.

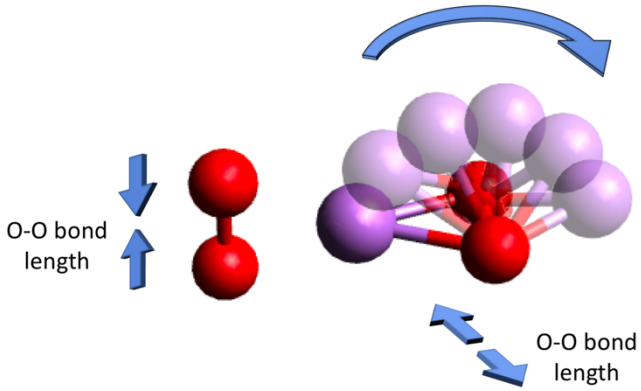

Figure 3: *Geometric motions of the atoms involved in reaction R9. The motion depicted brings the superoxide complex AmO_2^- to the reactants O_2+AmO_2^-: it consists in the simultaneous rotation of the metal atom from the center to the side of the complex and the concerted changes in the two O—O distances.*

The energies of the electronic states along the above reaction paths have been computed in vacuo for the 4 cations of Table 2 and are reported in Figure 4.

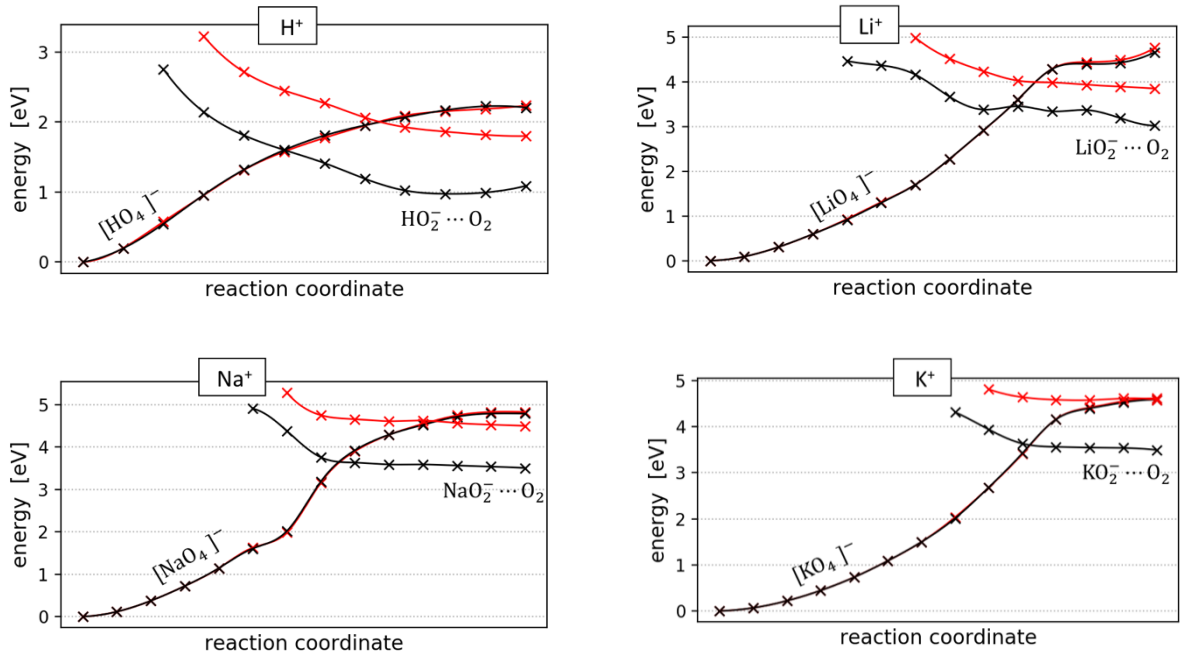

Figure 4: *Energies of the first 4 electronic states computed at the CASSCF/NEVPT2 level along the reaction path illustrated in Figure 3. The red lines correspond to singlet states and the black ones to triplet ones. On the left of the reaction coordinate there is the superoxide AmO_4^- complex, on the right the AmO_2^- peroxide plus O_2. The zero of the energies is set to be the optimized AmO_4^- complex.*

The reaction begins on the left with the AmO_4^- complex described by two almost degenerate electronic states (triplet and singlet, in black and red respectively). When moving toward the right, one of the two O—O distances decreases from 1.4 Å (superoxide) to 1.2 Å (molecular oxygen) while the other increases from 1.4 Å to 1.6 Å (peroxide). Along the evolution of the reaction, the two superoxide electronic states are increasingly and equally destabilized by the change in geometry while, at the same time, the peroxide electronic states are stabilized, and they cross the superoxide ones when going toward the products (right). The peroxide states have different energies depending on their multiplicity, with the triplet state being the more stable. The crossing point is approximately the point in which the electron transfer from one of the O_2 moiety to the other.

The important information that the data reported in Figure 4 tell us is that all the alkali metal reactions are dominated by thermodynamics with little or no kinetic barrier. Thus, the "transition state" (the crossing point) for Li, Na and K is a "late" one very similar in geometries and energies to the products.

3.2 The alkali-earth metals electronic energies

The disproportionation thermodynamics for the alkali-earth metals are summarized in Table 3. The reaction is significantly different from the alkali one. First of all, the initial superoxide in the reactant channel is a positively charged specie AeO_2^+. The reaction complex has the typical superoxide stoichiometry AeO_4 and is neutral. The final product, the peroxide, is also a neutral, AeO_2. We have limited our investigation to the reaction comprising only one alkali-earth metal because the association reaction of two positively charged superoxide molecules is impossible due to Coulomb repulsion. It is certainly possible to write a plausible reaction mechanism without including a free superoxide ion (O_2^-), but this would require additional atoms as to render the application of multiconfigurational techniques impractical.

With respect to the entrance channel $AeO_2^+ + O_2^-$ all alkali-earth metals reactions in the gas-phase are strongly exoergic. This effect is due to the huge energetic gain of the initial association process driven by the mutual Coulomb attraction in the reactant channel. When the Coulomb interaction is screened by the existence of a dielectric medium (in our case the SMD solvent model), the overall reaction energies are substantially reduced. For example, the association step in the case of Na, leads to -8 eV in the gas phase, but it is reduced to -2 eV in a sufficiently polar solvent such as CH_3CN.

The most interesting results in Table 3 are those for Mg and Ca, being Be too scarce on earth crust to expect commercial exploitations in battery prototypes. In both cases, the peroxide formation is strongly exoergic for low dielectric constant solvents, like diethyl ether: remarkably, in these cases even the reaction channel leading to the release of singlet oxygen is thermodynamically available. Increasing the dielectric constant as in acetonitrile, further reduce the Coulomb attraction and the singlet oxygen release shift upwards in energy and becomes endoergic.

The polarity of the solvent has a significant effect on the overall thermodynamics. Increasing the polarity significantly destabilize the products and makes the reaction less exoergic. In particular, for Na, the release of singlet oxygen from the disproportionation is expected to be an efficient process in the gas phase, but it requires 0.4 eV when the reaction occurs on CH_3CN. Despite the limited extent of our model, the calculation clearly points to the use of polar solvents as a mean to reduce the parasitic formation of singlet species.

Table 3: *NEVPT2/CASSCF energies for reaction R10. The data are reported for the triplet (ground state) multiplicity (normal fonts) and for the singlet multiplicity (excited state, bold fonts). All energies are referred to the reactant's energy:* $AeO_2^+ + O_2^-$.

Ae cation	Solvation	AeO_4	$AeO_2 \cdots O_2$	$AeO_2 + O_2$
Be^{2+}	gas	-11.51/**-11.52**	-9.01/**-7.98**	-8.60/**-7.64**
	Et_2O	-5.75/**-5.76**	-	-3.82/**-2.85**
	CH_3CN	-3.89/**-3.90**	-	-2.47/**-1.50**
Mg^{2+}	gas	-9.80/**-9.81**	-6.31/**-5.36**	-6.28/**-5.32**
	Et_2O	-3.76/**-3.76**	-	-1.85/**-0.89**
	CH_3CN	-1.99/**-1.99**	-	-0.63/**+0.33**
Ca^{2+}	gas	-8.17/**-8.17**	-5.50/**-4.55**	-5.45/**-4.49**
	Et_2O	-3.47/**-3.47**	-	-1.57/**-0.63**
	CH_3CN	-2.06/**-2.06**	-	-0.53/**+0.43**

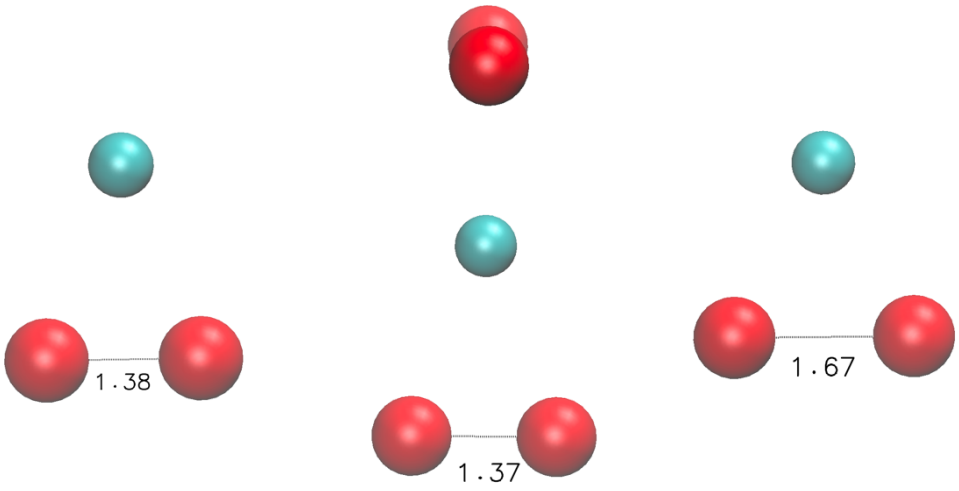

Figure 5: *MP2 geometries (in vacuo) of the stationary points along the R9 reaction for Mg^+ (cyan). In reading order: MgO_2^+ (superoxide), MgO_4 (reaction complex), MgO_2 (peroxide).*

The reactive path is exemplified in terms of molecular entities in Figure 5. Again, we see that the changes driving the reaction is the elongation of one of the O—O distances from the superoxide to the peroxide value. The reaction mechanism at play for the alkali-earth metals is analogous to what we have seen in Figure 4 for the alkali ones. The energies of the first 4 electronic states along the reaction path are shown in Figure 6 for Mg^{2+} and Ca^{2+} in the same fashion of Figure 3.

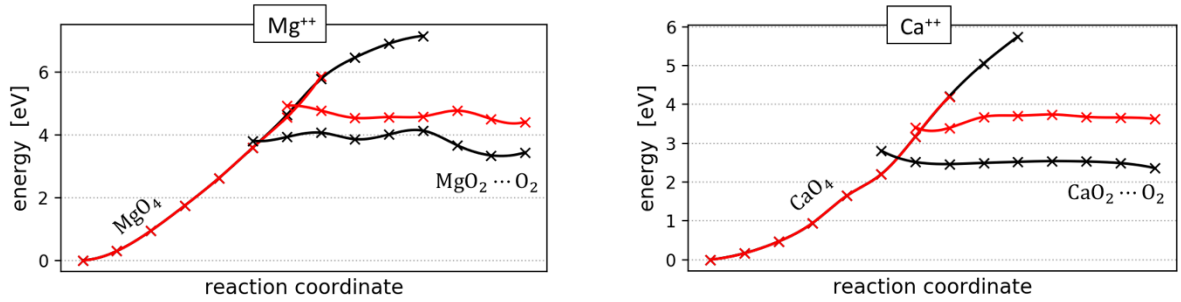

Figure 6: *Energies of the first 4 electronic states computed at the CASSCF/NEVPT2 level along the reaction path illustrated in Figure 3. The red lines correspond to singlet states and the black ones to triplet. On the left there is the superoxide AeO_4 complex, on the right the AeO_2 peroxide plus a neutral oxygen molecule. The zero of the energies is set to be the AeO_4 complex.*

As for the alkali metals, the points in which the electronic states cross are located almost at the same energy of the products states (on the right of the reaction coordinate). The reaction is therefore dominated by the thermodynamic energies: as soon as the reagent complex AeO_4 has

enough electronic energy to match the product one, it undergoes disproportionation to the peroxide state, exploiting the proximity (crossing) of the different electronic states.

3.3 The disproportionation reaction thermodynamics at 298K on the triplet ground state

To sketch a detailed thermodynamic description of reactions R8, R9 and R10, we have computed the ground state (the triplet electronic state) Gibbs free energies that account for entropic and zero-point-energy effects. The calculation is based on the evaluation of the vibrational states energies in the harmonic approximation at the stationary points. This, in turn, allows to write an approximate molecular partition function using perfect-gas formulae and the computation of the entropy change along the reaction path. The calculation of the free energies has been performed both in vacuo and in the solvent medium approximation, but we show here only the latter results which appear to be a more realistic description of the processes in an experimental setup. We must stress however that these data are based on two significant approximations: the vibrational degree of freedom is treated within the harmonic approximation and entropy and enthalpy are evaluated using perfect gas formulae.

We present the alkali reactions R8 and R9 in Figure 7 where, for the sake of completeness, we also report our data already presented in ref.[24] for the proton. In these figures, we also include the asymptotic fully dissociated initial state that, due to the Coulomb interaction, is located at a very high energy.

The free energy profile of reaction R8 (top panels of Figure 7), is characterized by a globally exoergic profile when including the fully ionic dissociation initial channel, but, at difference with the electronic energies in Table 1, the free energy gain from two isolated superoxide to the AmO_4 complex is now reduced due to the entropic negative contribution of the association process. In other words, considering free energies, the $2AmO_2$ channel is almost isoergic with the Am_2O_4 one.

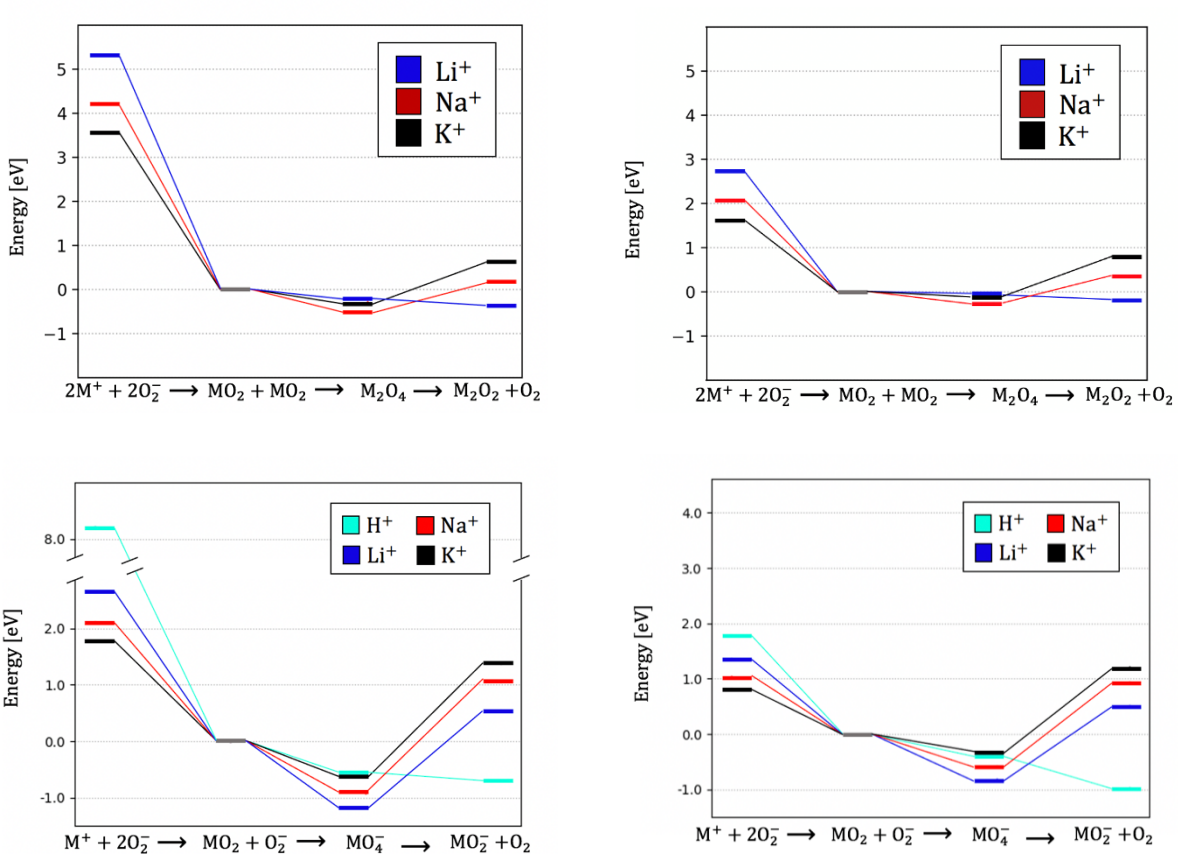

Figure 7: *Thermodynamic free energies of reactions R8 (top) and reaction R9 (bottom) in a solvent medium. Left panels are for Et_2O solvent, right ones for CH_3CN. Only the triplet (ground state) energies have been computed.*

The AmO_4 system evolves toward the peroxide product with an exoergic process for Li^+ and a moderately endoergic one for Na^+ and K^+. The entropy contribution due to the dissociative nature of the process (hence the release of molecular oxygen) facilitates the reaction, thus making the disproportionation reaction along the neutral path thermodynamically available with null-to-moderate energy content (between -0.2 and -0.4 eV for Li^+ and between 0.2 and 0.4 eV for Na^+ and between 0.6 and 0.8 K^+ depending on solvent polarity).

The thermodynamic path of reaction R9, the anionic one, reported in the bottom panels of Figure 9 is not altered in a substantial way by the introduction of entropic contributions with respect to the data of Table 2. The energy gain in passing from AmO_2+O_2^- is slightly reduced by the unfavorable entropic contribution, but the final evolution from AmO_4^- to the peroxide remains an endoergic process that requires ~2 eV in Et_2O and ~1 eV in CH_3CN.

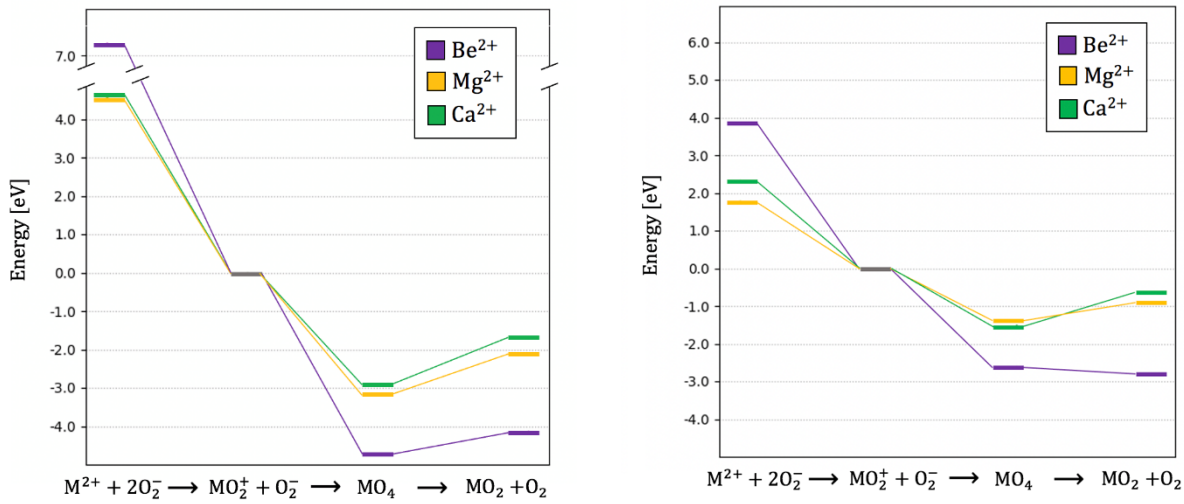

***Figure 8**: Thermodynamic free energies of reactions R10 in a solvent medium. Left panel is for Et_2O solvent, right one for CH_3CN. Only the triplet (ground state) energies have been computed.*

The situation for the alkali-earth metals in terms of free energies in solutions is illustrated in Figure 8. Apparently, the entropic contribution alters only slightly the situation described by the data of the electronic energies reported in Table 3. Both the Mg^{2+} and Ca^{2+} reactions remain exoergic with respect to the AeO_2^++O_2^- channel and the last step of the reaction that proceeds transforming the AeO_4 complex into the product is endoergic by about 1 eV in both Et_2O and CH_3CN. The comparison between reactions in small and large dielectric constant solvents (respectively left and right panels of figure 8) highlights the impact of medium polarity: the larger the dielectric constant the smaller the overall exoergic character of the process. It is important to underline that the stabilization of the asymptotic neutral products in high dielectric constant solvents is a common feature among alkaline and alkaline-earth metals superoxide disproportionation, and this trend has a remarkable impact on the possible release of singlet molecular oxygen.

If we compare the neutral processes pertaining to alkali and alkali-earth metals (i.e. the top panels of Figure 7 and those of Figure 8), we also notice that the reactive step that brings the superoxide (MO_2+MO_2) to peroxide (M_2O_2+O_2) is slightly endergonic for Na^+ and K^+, while it is slightly exergonic for Li^+. This thermodynamic landscape suggests that this path can be walked both ways in solution. The same process is strongly exergonic for both Mg^{2+} and Ca^{2+} and, therefore, the equilibrium is strongly shifted towards the formation of the products. A mitigation of the strong driving force to the formation of alkaline earth peroxides might be achieved for Mg^{2+} using solvents with very high dielectric constants (e.g. DMSO).

However, the disproportion reaction (from superoxide to peroxide) reversibility (from peroxide to superoxide) is unavoidably strictly related to the solubility of the neutral species involved. As an example, superoxides solubility is strongly altered by the dielectric constant of the solvent medium whereas all peroxides are always insoluble. [23] This means that the precipitation or aggregation of the insoluble species or their mutual solubility might strongly shift disproportions toward products formation, hence making the overall process irreversible.

4. Summary and concluding remarks

In this paper we shed light on the rather complicated mechanisms at play in the redox chemistry of metal-O_2 batteries. The nature of the molecules partaking to the reactions, due to their electronic states and to the coexistence of different multiplicities and electron arrangements requires the use of multiconfigurational calculation schemes. While on the one hand, this allows to provide quite accurate energies, on the other, it limits the size and the extent of the systems amenable to investigation. We have therefore identified three possible, few-atoms chemical processes by which the disproportionation of superoxide can occur in aprotic media, and we have evaluated their thermodynamic with and without solvent. The latter has been treated within a simple continuum approach approximation due to the aforementioned size limits of the present calculations.

Our calculations prove that, despite the apparent simplicity of the chosen reactions, their outcome is greatly influenced by several environmental factors which include the solvent polarity and the association state of superoxides. Many of the information provided by our calculations are entirely new especially those pertaining to alkaline earth metals and, as such they may provide very useful clues about the redox chemistry of metal-O_2 batteries and help in improving their technological implementation.

In order to summarize our results, in Figure 9, we sketch two mechanisms for alkaline and alkaline earth metals disproportionation reactions originating from the electrochemical reduction of molecular oxygen in aprotic media. Superoxide ions forms in aprotic electrochemical cells by the one-electron reduction of molecular oxygen molecules. Once formed, the superoxide anions have a strong driving force to combine with cations (see figures 7 and 8) to form neutral AmO_2 or positively charged AeO_2^+.

All superoxide species can undergo disproportionation by reaction with another superoxide specie: as already mentioned the direct interaction between superoxides anions is repulsive and therefore is allowed only by the presence of (partially) neutralizing cations.

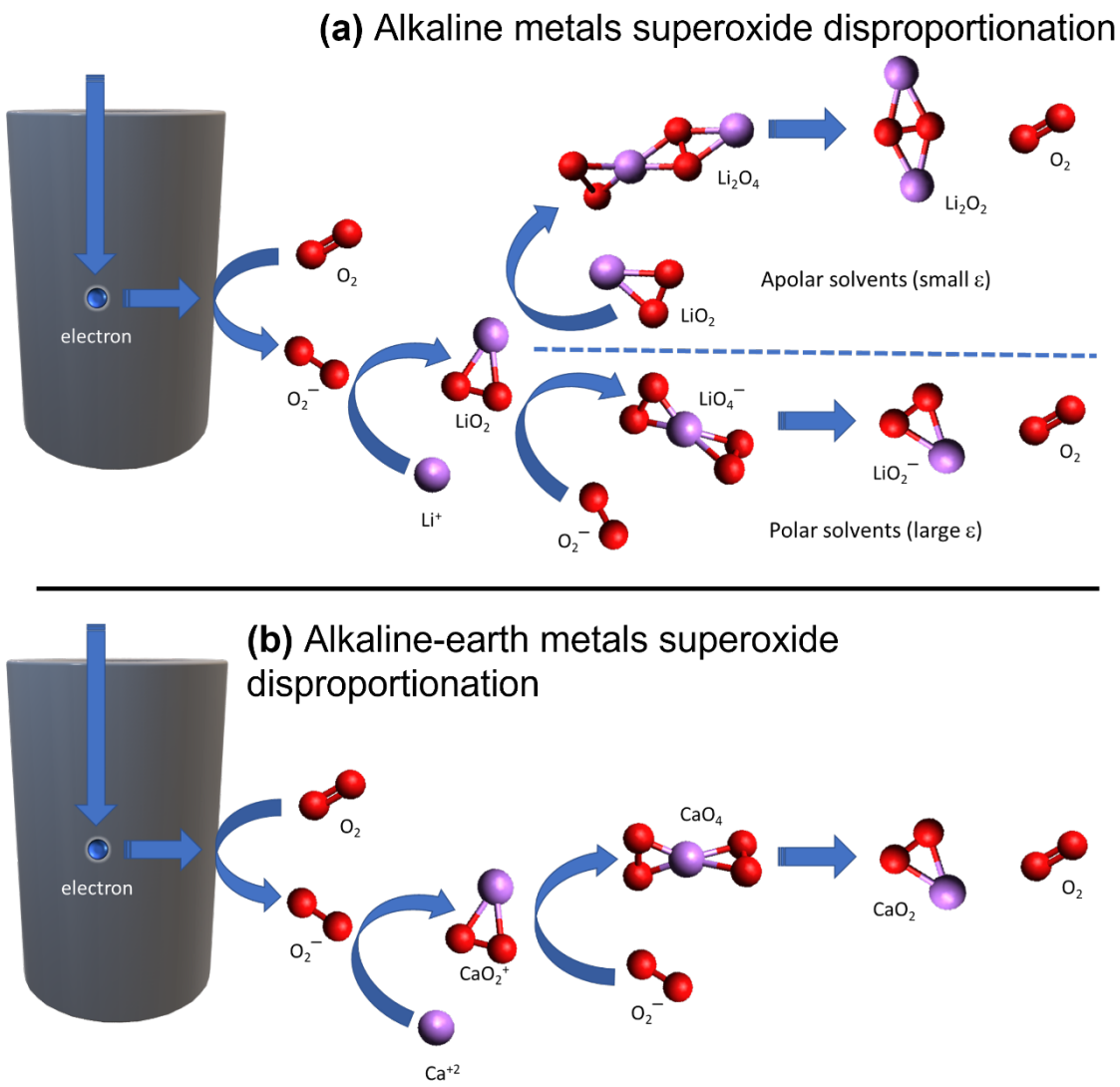

***Figure 9**: Visual representation of the chemical mechanisms of disproportionation of (a) alkaline metals (lithium in the figure) and (b) alkaline-earth metals superoxides (calcium in the figure) originated from the electrochemical reduction of molecular oxygen in aprotic media.*

For alkaline ions the disproportionation can be mediated by one or two cations and therefore the dielectric constant of the solvent drives the ionicity of the reaction. In apolar or low dielectric constant solvent, neutral superoxides dimerize to from neutral Am_2O_4 complexes that can easily release oxygen molecules (see the figure 7a). Consequently, the release of singlet oxygen in Am-O_2 batteries in low dielectric constant solvents is thermodynamically feasible. On the other hand, in

polar solvents spontaneous disproportionation mediated by one single alkaline ion are hindered by the increase of the Gibbs energy of reaction to release molecular oxygen. Therefore, the increase of the dielectric constant of the solvent media hinders the singlet oxygen molecular release by disproportionation mediated by alkaline ions.

Turning to alkaline-earth ion promoted disproportionation, it can be mediated by one cation only since it is strongly unlikely that two AeO_2^+ species dimerizes, whereas AeO_2^+ can easily combine with another O_2^- to form the AeO_4 complex. Once formed, the neutral AeO_4 specie can easily undergo disproportionation driven by a favorable thermodynamics in solvents with large dielectric constants. Low dielectric constant solvents increase the Gibbs energy of the latter reaction to values larger than 1 eV for both Mg^{2+} and $Ca^{2+,}$ thus making negligible any disproportionation at room temperature. Overall, the increase of the dielectric constant of the solvent media facilitates the singlet oxygen molecular release by disproportionation mediated by alkaline-earth ions.

Acknoledgements

S.B. and E.B wish to thank the University of Rome la Sapienza for the financial support through the projects RM120172A46A7608, RG1181643265D950 and RM11916B658EF0BA.

References

1 P. G. Bruce, S. Freunberger, L. J. Hardwick and J.-M. Tarascon, Li-O_2 and Li-S batteries with high energy storage., *Nat. Mater.*, 2012, **11**, 19–29.

2 P. G. Imanishi, N.; Luntz, A.; Bruce, *The Lithium Air Battery: Fundamentals*, Springer, New York (USA), 2014.

3 K. Song, D. A. Agyeman, M. Park, J. Yang and Y.-M. Kang, High-Energy-Density Metal–Oxygen Batteries: Lithium–Oxygen Batteries vs Sodium–Oxygen Batteries, *Adv. Mater.*, 2017, **29**, 1606572.

4 P. Reinsberg, C. J. Bondue and H. Baltruschat, Calcium-oxygen batteries as a promising alternative to sodium-oxygen batteries, *J. Phys. Chem. C*, 2016, **120**, 22179–22185.

5 T. Shiga, Y. Kato and Y. Hase, Coupling of nitroxyl radical as an electrochemical charging catalyst and ionic liquid for calcium plating/stripping toward a rechargeable calcium-oxygen battery, *J. Mater. Chem. A*, 2017, **5**, 13212–13219.

6 J. G. Smith, J. Naruse, H. Hiramatsu and D. J. Siegel, Theoretical Limiting Potentials in Mg/O_2 Batteries, *Chem. of Mater.*, 2016, **28**, 1390–1401.

7 G. Vardar, E. G. Nelson, J. G. Smith, J. Naruse, H. Hiramatsu, B. M. Bartlett, A. E. S. Sleightholme, D. J. Siegel and C. W. Monroe, Identifying the Discharge Product and Reaction Pathway for a Secondary Mg/O 2 Battery , *Chem. Mater.*, 2015, **27**, 7564–7568.

8 M. Balaish, A. Kraytsberg and Y. Ein-Eli, A critical review on lithium-air battery electrolytes, *Phys. Chem. Chem. Phys.*, 2014, **16**, 2801–2822.

9 M. Carboni, A. G. Marrani, R. Spezia and S. Brutti, 1,2-Dimethoxyethane Degradation Thermodynamics in Li−O_2 Redox Environments, *Chem. Eur. J.*, 2016, **22**, 17188–17203.

10 M. Carboni, A. G. Marrani, R. Spezia and S. Brutti, Degradation of LiTfO / TEGME and LiTfO / DME Electrolytes in Li-O_2 Batteries, *J. Electrochem. Soc.*, 2018, **165**, 1–9.

11 A. I. Belova, D. G. Kwabi, L. v. Yashina, Y. Shao-Horn and D. M. Itkis, Mechanism of Oxygen Reduction in Aprotic Li–Air Batteries: The Role of Carbon Electrode Surface Structure, *J. Phys. Chem. C*, 2017, **121**, 1569–1577.

12 K. C. Lau, R. S. Assary, P. Redfern, J. Greeley and L. A. Curtiss, Electronic Structure of Lithium Peroxide Clusters and Relevance to Lithium–Air Batteries, *J.Phys. Chem. C*, 2012, **116**, 23890–23896.

13 K. C. Lau, L. A. Curtiss and J. Greeley, Density Functional Investigation of the Thermodynamic Stability of Lithium Oxide Bulk Crystalline Structures as a Function of Oxygen Pressure, *J. Phys. Chem. C*, 2011, **115**, 23625–23633.

14 N. Kumar, M. D. Radin, B. C. Wood, T. Ogitsu and D. J. Siegel, Surface-mediated solvent decomposition in Li-Air batteries: Impact of peroxide and superoxide surface terminations, *J. Phys. Chem. C*, 2015, **119**, 9050–9060.

15 U. Das, K. C. Lau, P. C. Redfern and L. A. Curtiss, Structure and Stability of Lithium Superoxide Clusters and Relevance to Li–O_2 Batteries, *J. Phys. Chem. Lett.*, 2014, **5**, 813–819.

16 N. Mahne, O. Fontaine, M. Ottakam Thotiyl, M. Wilkening and S. Freunberger, Mechanism and performance of lithium-oxygen batteries – a perspective, *Chem. Sci.*, 2017, **8**, 6716–6729.

17 M. Carboni, S. Brutti and A. G. Marrani, Surface Reactivity of a Carbonaceous Cathode in a Lithium Triflate/Ether Electrolyte-based Li–O_2 Cell., *ACS Appl. Mater. Interfaces,* 2015, **7**, 21751–21762.

18 D. Giacco, M. Carboni, S. Brutti and A. G. Marrani, Noticeable Role of TFSI – Anion in the Carbon Cathode Degradation of Li–O_2 Cells, *ACS Appl. Mater. Interfaces*, 2017, **9**, 31710–31720.

19 S. A. Freunberger, Y. Chen, N. E. Drewett, L. J. Hardwick, F. Bardé and P. G. Bruce, The lithium-oxygen battery with ether-based electrolytes, *Angew. Chem. Int. Ed.*, 2011, **50**, 8609–8613.

20 C. P. Andrieux, P. Hapiot and J. michel Saveant, Mechanism of Superoxide Ion Disproportionation in Aprotic Solvents, *J. Am. Chem. Soc.*, 1987, **109**, 3768–3775.

21 Y. Che, M. Tsushima, F. Matsumoto, T. Okajima, K. Tokuda and T. Ohsaka, Water-induced disproportionation of superoxide ion in aprotic solvents, *J. Phys. Chem.*, 1996, **100**, 20134–20137.

22 J. M. Aubry, J. Rigaudy, C. Ferradini and J. Pucheault, A Search for Singlet Oxygen in the Disproportionation of Superoxide Anion, *J. Am. Chem. Soc.*, 1981, **103**, 4965–4966.

23 E. Mourad, Y. K. Y. K. Petit, R. Spezia, A. Samojlov, F. F. F. Summa, C. Prehal, C. Leypold, N. Mahne, C. Slugovc, O. Fontaine, S. Brutti and S. A. S. A. Freunberger, Singlet oxygen from cation driven superoxide disproportionation and consequences for aprotic metal-O_2 batteries, *Energy Environ.l Sci.*, 2019, **12**, 2559–2568.

24 A. Pierini, S. Brutti and E. Bodo, Superoxide Anion Disproportionation Induced by Li^+ and H^+ : Pathways to $^1O_2$ Release in Li−O_2 Batteries, *ChemPhysChem*, 2020, **21**, 2060–2067.

25 N. Mahne, S. E. Renfrew, B. D. McCloskey and S. A. Freunberger, Electrochemical Oxidation of Lithium Carbonate Generates Singlet Oxygen, *Angew. Chem. Int. Ed.,* 2018, **57,** 5529-5533.

26 N. Mahne, B. Schafzahl, C. Leypold, M. Leypold, S. Grumm, A. Leitgeb, G. A. Strohmeier, M. Wilkening, O. Fontaine, D. Kramer, C. Slugovc, S. M. Borisov and S. A. Freunberger, Singlet oxygen generation as a major cause for parasitic reactions during cycling of aprotic lithium–oxygen batteries, *Nat. Energy*, 2017, **2**, 17036.

27 J. Wandt, P. Jakes, J. Granwehr, H. A. Gasteiger and R.-A. Eichel, Singlet Oxygen Formation during the Charging Process of an Aprotic Lithium-Oxygen Battery, *Angew. Chem. Int. Ed.*, 2016, **128**, 7006–7009.

28 L. Schafzahl, N. Mahne, B. Schafzahl, M. Wilkening, C. Slugovc, S. M. Borisov and S. A. Freunberger, Singlet Oxygen during Cycling of the Aprotic Sodium–O_2 Battery, *Angew. Chem. Int. Ed.*, 2017, **56**, 15728–15732.

29 P. P. Bawol, P. H. Reinsberg, A. Koellisch-Mirbach, C. J. Bondue and H. Baltruschat, The Oxygen Reduction Reaction in Ca^{2+}-Containing DMSO: Reaction Mechanism, Electrode Surface Characterization, and Redox Mediation**, *ChemSusChem*, 2021, **14**, 428–440.

30 F. Neese, Software update: the ORCA program system, version 4.0, *WIREs Comp. Molec. Sci.*, 2018, **8**, 1327.

31 S. Grimme, Improved second-order Møller–Plesset perturbation theory by separate scaling of parallel- and antiparallel-spin pair correlation energies, *J. Chem. Phys.*, 2003, **118**, 9095.

32 C. Angeli, R. Cimiraglia, S. Evangelisti, T. Leininger and J.-P. Malrieu, Introduction of n-electron valence states for multireference perturbation theory, *J. Chem. Phys.*, 2001, **114**, 10252.

33 C. Angeli, R. Cimiraglia and J.-P. Malrieu, n-electron valence state perturbation theory: A spinless formulation and an efficient implementation of the strongly contracted and of the partially contracted variants, *J. Chem. Phys.*, 2002, **117**, 9138.

34 A. Pierini, S. Brutti and E. Bodo, *Reactive pathways toward parasitic release of singlet oxygen in metal-air batteries*, npj Comp. Mat., 2021, **7**, 126.

35 A. V. Marenich, C. J. Cramer and D. G. Truhlar, Universal solvation model based on solute electron density and on a continuum model of the solvent defined by the bulk dielectric constant and atomic surface tensions, *J. Phys. Chem. B*, 2009, **113**, 6378–6396.